# Identification of discrete functional subregions of the human periaqueductal gray

Ajay B. Satpute[a,1], Tor D. Wager[b], Julien Cohen-Adad[c], Marta Bianciardi[d], Ji-Kyung Choi[d], Jason T. Buhle[e], Lawrence L. Wald[d], and Lisa Feldman Barrett[a,f]

[a]Department of Psychology, Northeastern University, Boston, MA, 02115; [b]Department of Psychology and Neuroscience, University of Colorado at Boulder, Boulder, CO 80309; [c]Department of Electrical Engineering, École Polytechnique de Montréal, Montreal, QC, Canada H3T 1J4; Departments of [d]Radiology and [f]Psychiatry, Athinoula A. Martinos Center for Biomedical Imaging, Massachusetts General Hospital and Harvard Medical School, Charlestown, MA 02129; and [e]Department of Psychology, Columbia University, New York, NY, 10027

Edited by Marcus E. Raichle, Washington University in St. Louis, St. Louis, MO, and approved September 9, 2013 (received for review March 30, 2013)

**The midbrain periaqueductal gray (PAG) region is organized into distinct subregions that coordinate survival-related responses during threat and stress [Bandler R, Keay KA, Floyd N, Price J (2000) *Brain Res* 53 (1):95–104]. To examine PAG function in humans, researchers have relied primarily on functional MRI (fMRI), but technological and methodological limitations have prevented researchers from localizing responses to different PAG subregions. We used high-field strength (7-T) fMRI techniques to image the PAG at high resolution (0.75 mm isotropic), which was critical for dissociating the PAG from the greater signal variability in the aqueduct. Activation while participants were exposed to emotionally aversive images segregated into subregions of the PAG along both dorsal/ventral and rostral/caudal axes. In the rostral PAG, activity was localized to lateral and dorsomedial subregions. In caudal PAG, activity was localized to the ventrolateral region. This shifting pattern of activity from dorsal to ventral PAG along the rostrocaudal axis mirrors structural and functional neurobiological observations in nonhuman animals. Activity in lateral and ventrolateral subregions also grouped with distinct emotional experiences (e.g., anger and sadness) in a factor analysis, suggesting that each subregion participates in distinct functional circuitry. This study establishes the use of high-field strength fMRI as a promising technique for revealing the functional architecture of the PAG. The techniques developed here also may be extended to investigate the functional roles of other brainstem nuclei.**

brain stem | neuroimaging | emotion | high-resolution

The periaqueductal gray (PAG) is a small tube-shaped region of the midbrain involved in survival-related responses and homeostatic regulation important for affective responses and stress (1–3). Subregions of the PAG underlie distinct, coordinated behavioral responses to threat. For example, stimulation in the lateral/dorsolateral portion produces active-coping responses (e.g., "fight" or "flight") that involve increasing heart rate and arterial pressure, redistribution of the blood to the limbs, and a fast-acting, nonopioid-mediated analgesia. Stimulation in the ventrolateral portion produces passive-coping responses (i.e., disengagement, freezing) that involve reduced heart rate, decreased reactivity to the environment, and a longer-term, opioid-mediated analgesic response. These responses occur even when inputs to PAG from the cortex are severed (1, 4).

The considerable animal literature on the critical role of the PAG in coordinating emotional responses has led to a surge of interest in studying the PAG in humans. The PAG plays a central role in neurobiologically inspired theories of human emotion (5), the neural circuitry underlying depression and anxiety (3, 6), autonomic regulation (7), and pain (8–11). To examine PAG function in humans, researchers have relied primarily on functional MRI (fMRI). To date, dozens of human neuroimaging studies have observed increased activation in the vicinity of the PAG during administration of painful and aversive stimuli (8, 12–16) and across a variety of emotional states (17).

Unfortunately however, standard fMRI is fundamentally limited in its resolution, making it uncertain which fMRI results lie in the PAG and which lie in other nearby nuclei. The overarching issue is size and shape. The PAG is small and is shaped like a hollow cylinder with an external diameter of ∼6 mm, a height of ∼10 mm, and an internal diameter of ∼2–3 mm. The cerebral aqueduct, which runs through the middle, can prevent detecting activations within the PAG [type II errors (18)] and also can create artificial activations that appear to be in the PAG but are not [type I errors (19)], making the PAG particularly challenging to image among the subcortical nuclei. Standard smoothing and normalization procedures, even with high-resolution scanning, incorporate signal from the aqueduct (Fig. 1). This signal can be overpowering. The variability of signal in the aqueduct can be an order of magnitude greater than that of the surrounding PAG. (Figs. S1 and S2).

Standard neuroimaging techniques also are fundamentally limited in capturing the remarkable functional organization that is internal to the PAG. In addition to being differentiated into columns (1, 4), the PAG also is organized rostrocaudally. In caudal PAG, neurons that contain endogenous opioids and neuropeptides involved in nonopioid analgesia are concentrated in the ventrolateral columns, whereas in rostral PAG this concentration is greater in the lateral and dorsomedial columns (20, 21). Mirroring this distribution, administration of anxiogenic drugs produces greater neural activity in caudal, ventrolateral PAG and rostral, dorsolateral PAG [as measured from c-Fos

## Significance

**The periaqueductal gray is a brainstem region that is critical for autonomic regulation and for defensive responses (e.g., "fight," "flight," "freeze"). It has been studied extensively in rodents and cats, but less is known about the human periaqueductal gray. The small size and shape of the periaqueductal gray makes it challenging to study using standard noninvasive MRI techniques. We used a high-field strength magnet to examine this region at high resolution while participants viewed emotionally aversive or neutral images. Emotion-related functional activity was concentrated in particular subregions and in ways that are consistent with neurobiological observations in nonhuman animals. This study establishes a technique to uncover the functional architecture of the periaqueductal gray in humans.**

Author contributions: A.B.S., T.D.W., J.T.B., L.L.W., and L.F.B. designed research; A.B.S., J.C.-A., M.B., and J.-K.C. performed research; J.C.-A., and L.L.W. contributed new reagents/analytic tools; A.B.S. analyzed data; and A.B.S., T.D.W., J.C.-A., M.B., J.-K.C., J.T.B., L.L.W., and L.F.B. wrote the paper.

The authors declare no conflict of interest.

This article is a PNAS Direct Submission.

[1]To whom correspondence should be addressed. E-mail: a.satpute@neu.edu.

This article contains supporting information online at www.pnas.org/lookup/suppl/doi:10.1073/pnas.1306095110/-/DCSupplemental.

NEUROSCIENCE

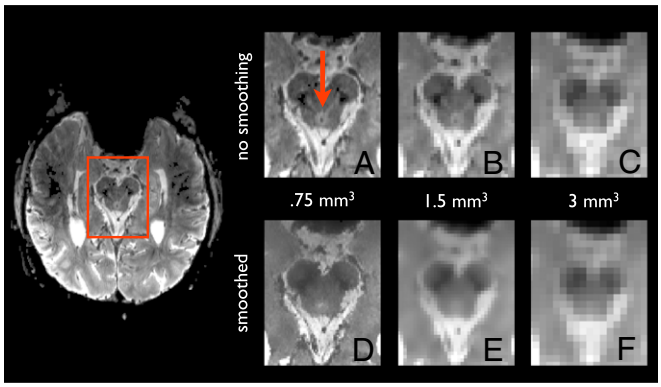


**Fig. 1.** The PAG imaged at high resolution. The transaxial slice on the left shows the PAG from a functional scan at ultra-high field strength (7-T) and high resolution (0.75 mm isotropic). Scanning the PAG at lower resolutions prevents clear separation of the PAG from the aqueduct and surrounds. (*A*) The mean functional image for a single run at the 0.75-mm isotropic resolution used in this study shows the PAG crisply as indicated by the red arrow. (*B*) Downsampling the image to a resolution of 1.5 mm isotropic begins to blur the boundary between the PAG and its surrounds because of partial-volume effects. (*C*) Further downsampling the image to a resolution of 3 mm isotropic eliminates the ability to distinguish PAG from the aqueduct with any degree of confidence. (*D–F*) Smoothing with a standard 4-mm kernel further increases the partial-volume effects that blend signal from PAG with the aqueduct and surrounds, as shown for 0.75 mm isotropic (*D*), 1.5 mm isotropic (*E*), and 3 mm isotropic (*F*) resolutions. Most neuroimaging studies use a 3-mm isotropic resolution with a 4-mm or higher smoothing kernel. We addressed these issues by separating PAG voxels from the aqueduct before additional image processing (i.e., using the image shown in *A*) so that only voxels within the PAG are incorporated into later stages of analysis. The top of the transaxial image corresponds to the anterior portion of the head; the bottom corresponds to the posterior portion of the head.

expression (22)]. Connections from the central nucleus of the amygdala terminate more extensively in lateral and dorsal rostral PAG and ventrolateral caudal PAG (23). The ability to resolve which of these circuits is involved in a given behavior is crucial for understanding the implications of PAG activity in a given situation and for mapping homologies across species.

Resolving activity to subregions of the PAG requires greater precision than provided by any study to date. Indeed, the overwhelming majority of previous studies have used 1.5- or 3-T MRI systems that typically cannot exceed an isotropic resolution of 1.5–2 mm without incurring significant losses in the signal-to-noise ratio (SNR) and significant increases in image distortion. This resolution already introduces substantial partial-volume effects (Fig. 1) that merge signal from the PAG with the exceedingly variable signal in the aqueduct (Fig. S2). Standard intersubject normalization and smoothing procedures that generally increase SNR but diminish localization accuracy further aggravate these issues. Ultimately, standard fMRI techniques—even those using high-resolution scanning—are incapable of capturing the functional organization of the PAG in humans.

To overcome these obstacles, we used ultra-high field (7-T) fMRI combined with 32-channel parallel imaging (24), which can boost sensitivity by as much as an order of magnitude compared with low-field strength magnets (1.5–3 T) and volume coils (25). Higher-field strength magnets also provide greater sensitivity to the susceptibility effects that underlie the blood-oxygenation level–dependent (BOLD) signal measured in fMRI (26) and greater sensitivity to microvasculature (27, 28). At a nominal voxel resolution of 0.75 mm isotropic (Fig. 1*A*), we isolated the PAG directly from the functional scans and separated activity in the PAG from activity in the aqueduct (Fig. S1).

We examined activity in the PAG while participants viewed aversive images (29), which included images of burn victims, gory injuries, and other content related to threat, harm, and loss, or while they viewed neutral images. Although prior studies have demonstrated activity in the vicinity of the PAG during the viewing of aversive images (15), we first tested whether the PAG definitively showed greater activity during to these images when signal was separated from the aqueduct and surrounding brainstem nuclei. Next, we used two approaches to test whether activity was localized to subregions of the PAG. In one approach, we segmented the PAG along dorsal/ventral and rostral/caudal divisions and examined whether activity was localized within specific segments. In a second but related approach, we performed analyses on a voxel-by-voxel basis to test whether high-field strength imaging can map the functional architecture of PAG at the voxel level. Given that discrete voxels identified in this approach necessarily would reside within just a few millimeters of each other, we performed a factor analysis to discover whether they carried similar or unique information during emotional responses.

## Results

**Activation in PAG During Aversive-Image Viewing.** In a first analysis, we averaged signal within the PAG and found that activity was greater during the viewing of highly aversive images than during the viewing of neutral images [$t$ (10) = 3.538, $P < 0.005$]. There were no effects in the aqueduct [$t$ (10) = 0.348, $P < 0.75$]. This finding provides definitive evidence of PAG activation during the presentation of aversive images.

**Identifying Discrete Functional Subregions of PAG During Aversive-Image Viewing: Mask-Based Segmentation.** Using the known internal organization of the PAG in nonhuman animals, we tested whether activity in subregions of human PAG was localized to particular columns, within particular rostrocaudal segments, or both. First, we implemented a customized normalization procedure to align voxels in the PAG into a common subject space without including signal from the aqueduct or surrounding tissue (Fig. S1). We then divided the PAG radially (six segments radially divided along dorsoventral and left/right axes) and along the rostrocaudal axis (six segments: three rostral and three caudal) and averaged activity across voxels within these segments for each subject (Fig. 2*B*).

A repeated-measures ANOVA across picture type (aversive vs. neutral), radial locations, and longitudinal segments produced a significant three-way interaction [$F$ (25, 250) = 2.173, $P < 0.0015$]. These results indicate that differences in activity during the viewing of aversive vs. neutral pictures depended on the interaction between radial and longitudinal segments. No other effects reached significance (aside from the main effect of picture type). We further tested for lateralization in left and right lateral and ventrolateral PAG using a second repeated-measures ANOVA and observed no significant lateralization effects ($P >$ 0.35 for all cases in which lateralization was a factor).

Unpacking the three-way interaction showed that activations followed a spiral-like pattern similar to that observed in nonhuman animals for the distribution of analgesia-related peptides (20, 21), c-Fos expression upon anxiogenic drug administration (22), and connections to PAG from the central nucleus of the amygdala (23). Although exactly where a transition from caudal ventrolateral PAG to rostral lateral/dorsomedial PAG may occur remains unclear (particularly in humans), an approximation using the findings in nonhuman animals suggests that each extends about halfway along the rostrocaudal axis.

Averaging within the rostral and caudal segments of the PAG, we found that the difference in activity during the viewing of gory vs. neutral images was greater in the rostral half in dorsomedial PAG [$t$ (10) = 3.19, $P = 0.0096$] and lateral PAG [$t$ (10) = 3.06,

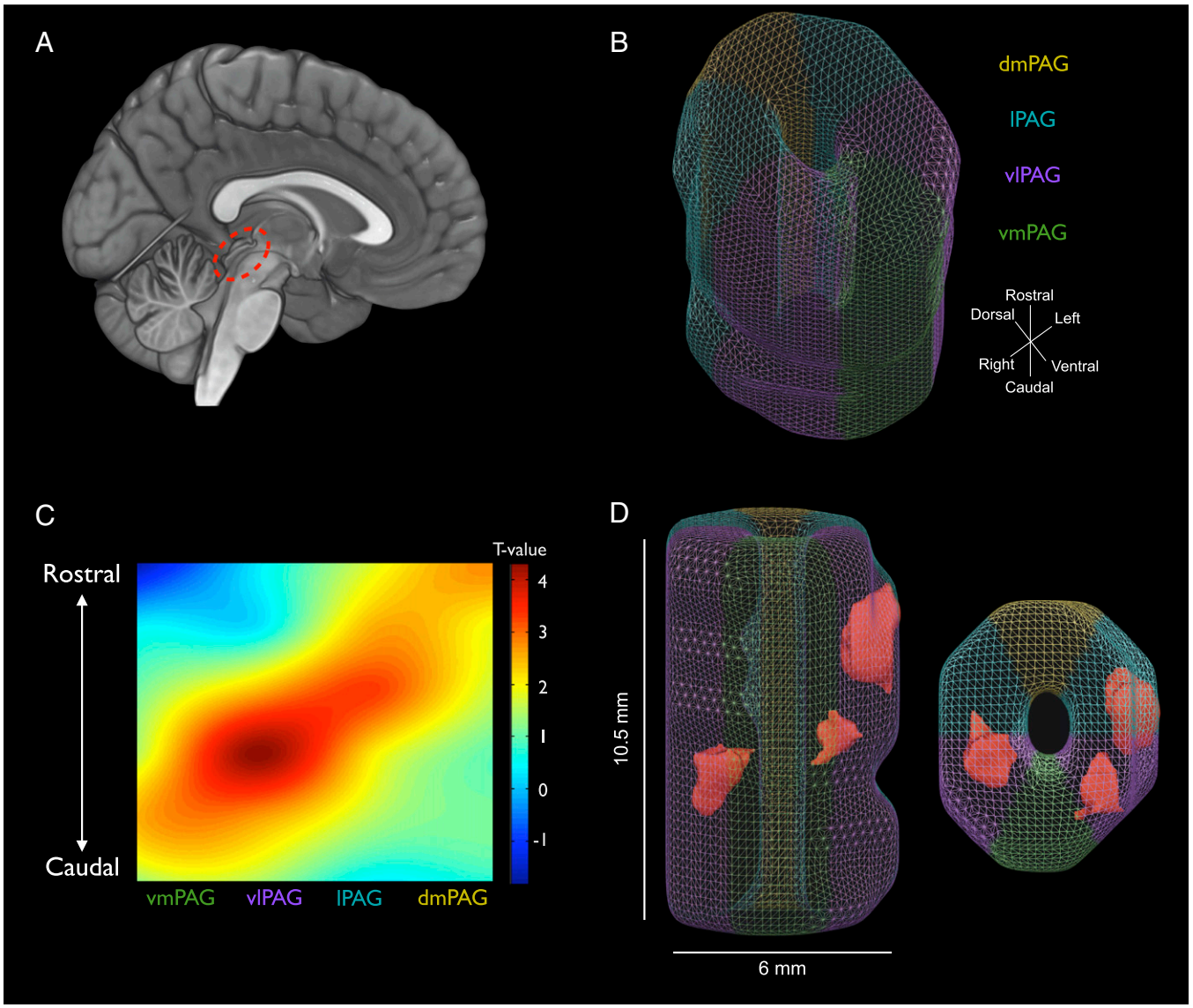


**Fig. 2.** Distribution of functional activity in PAG subregions during aversive-image viewing. (*A*) The sagittal brain rendering illustrates the location of the PAG on a canonical brain image (using MRIcroGL software). (*B*) A sample-specific PAG template was generated directly from the functional scans (see Fig. S1 for details). The template was divided into six radial segments for the dorsomedial PAG (dmPAG; highlighted in mustard), the lateral PAG (lPAG; light blue), the ventrolateral PAG (vlPAG; purple), and the ventromedial PAG (vmPAG; green). It was divided further into six rostrocaudal or longitudinal segments that are not depicted but which consisted of slabs that were perpendicular to the radial segments. (*C*) The plot illustrates the pattern of *t* scores across PAG segments for the difference in neural activity during the viewing of aversive relative to neutral images. Radial locations of segments are plotted on the *x*-axis, collapsed across laterality (which showed no significant effects). Longitudinal locations of segments are plotted on the *y*-axis. Segments were interpolated to illustrate the pattern in the plot. The plot shows that activity was organized both radially and rostrocaudally. From caudal to rostral PAG, activity transitioned from ventrolateral PAG to lateral and dorsomedial PAG. This spiral-like pattern mirrors neuroanatomical observations in nonhuman animals (see main text). (*D*) The figure illustrates results from voxelwise analyses comparing activity during the viewing of aversive relative to neutral images. Although mask-based segmentation approaches as presented in *B* and *C* rely on assuming a particular structural organization before identifying functional activity within it, voxelwise analyses are important for studies aiming to discover novel functional architectures of human PAG. Significant clusters were observed in the rostral lateral PAG and in caudal ventrolateral PAG ($P < 0.05$, corrected for the entire PAG volume; Fig. S3 shows mean time-course plots). The voxelwise analyses display the utility of high-field strength imaging for detecting activity in specific voxels within the PAG.

$P = 0.012$] but not in the caudal half [$t$ (10) = 1.03, $P = 0.33$, and $t$ (10) = 1.44, $P = 0.18$, respectively]. In contrast, ventrolateral PAG showed the opposite pattern, with greater activity in the caudal half [$t$ (10) = 3.08, $P = 0.012$] but not in the rostral half [$t$ (10) = 1.21, $P = 0.25$]. Activity in ventromedial PAG paralleled that in ventrolateral PAG numerically, but differences in caudal PAG did not reach significance [caudal: $t$ (10) = 2.07, $P = 0.065$; rostral: $t$ (10) = -0.039, $P = 0.97$, respectively]. The pattern of results is illustrated in Fig. 2*C*.

**Identifying Discrete Functional Subregions of PAG During Aversive-Image Viewing: Voxelwise Analyses.** Voxelwise analyses across the entire PAG volume complement the mask-based analyses in two ways. First, in assessing the ability of high-field strength and high-resolution neuroimaging to identify the functional properties of the human PAG, it is important to determine whether activity in the PAG can be identified on the voxel level. This approach allows investigators to discover, rather than stipulate, what the functional organization of the human PAG may be and supports

the use of data-driven voxelwise analyses to examine PAG function in future studies. Second, although mask-based approaches typically are more powerful statistically, they also introduce partial-volume effects that can merge distinct signals when the underlying neuroanatomy can only be approximated. Here, voxelwise analyses serve to mitigate these limitations (at least to the resolution of the voxel) and are less likely to merge variability arising from distinct sources.

We performed voxelwise analyses by comparing activity during the viewing of aversive images relative to neutral images across the PAG volume (corrected for multiple comparisons using the FMRIB Software Library threshold-free cluster estimation tool, tfce). As shown in Fig. 2*D*, the results showed three distinct clusters. The mesh coloring in the figure is provided for visual comparison with the mask-based analyses using segments, but the voxelwise analyses did not incorporate these segments in the analysis. Subregions were located in the left rostral lateral region [$t$ (10) = 6.03, $P < 0.001$, $P_{tfce} < 0.05$] and in the caudal ventrolateral region (bilaterally, left: $t$ (10) = 5.17, $P < 0.001$, $P_{tfce} < 0.05$; right: $t$ (10) = 5.81, $P < 0.001$, $P_{tfce} < 0.05$). These findings show that functional activity was localized to discrete clusters at the voxel level. Mean time-course plots for the three peak voxels are presented in Fig. S3.

The clusters we identified were only a few millimeters apart. Hence, we examined whether they showed differential patterns of variability, which would suggest that they participate in distinct functional circuits, or whether they showed similar patterns of variability, which would suggest that they do not participate in distinct functional circuits. Specifically, we examined how activation in these regions varied from each other and with reports of emotional experience in an exploratory factor analysis. For each participant, we extracted the average parameter estimate from 0.75-mm spheres centered on the peak voxel for each cluster during aversive- vs. neutral-image viewing and submitted these scores along with the differences in self-reported emotional experience for aversive vs. neutral images to an exploratory factor analysis. We reasoned that if activation in the lateral and ventrolateral PAG clusters participated in the same functional circuit, they would load on a single factor or at least similarly across factors. However, if activation in these clusters contributed unique variability during affective responses, then more than one factor would be required to explain their variability, and they would load on different factors.

Three factors with eigenvalues above 1 were obtained in the solution (Table S1). These factors explained 35, 24, and 18% of the variability. Intercorrelations among factors were low (maximal $r = 0.17$), indicating they were likely to be independent. An examination of the factor loadings showed that instead of loading similarly across factors, each PAG cluster loaded primarily on a separate factor and with different emotional experiences. Factor 1 involved the right caudal ventrolateral PAG ($\lambda = -0.73$) and the emotions disgust, arousal, and fear (all $\lambda > 0.72$). Factor 2 involved the left caudal ventrolateral PAG ($\lambda = -0.85$) and anger ($\lambda = 0.89$). Factor 3 involved the left rostral lateral PAG ($\lambda = 0.82$) and sadness ($\lambda = 0.92$). All other loadings between PAG regions or emotions and factors were less than 0.4 (Table S2). These results suggest that the PAG clusters contribute to different functional circuits. Indeed, pairwise correlations between PAG regions were low and revealed no significant relationships (all $P$s $> 0.25$; regardless of sign, maximal $r = -0.18$). Overall, these results indicate that the PAG subregions identified in voxelwise analyses carried functionally different sources of variability during affective responses.

Importantly, this study was not designed to address precisely which regions of the PAG are related to precisely which kinds of emotional experiences. Indeed, making strong predictions about the relationship between self-reported experience of emotions and animal behavioral responses during threat may be premature. Self-reports of emotional states are not diagnostic of nor do they show one-to-one correspondence with specific behavioral actions in humans or in nonhuman animals (studies reviewed in refs. 30–32). As such, aligning behaviors in animal research with emotional experiences in human research is not likely to be strongly justified. The high-resolution imaging techniques developed in this study may help reveal what relationships are present in behavior, experience, and activation of PAG subregions during emotion in future experiments.

Nonetheless, the shared loadings we observed between PAG activity and emotional experiences may be useful for formulating hypotheses in future research in humans. For descriptive purposes, we computed pairwise correlations between emotional experiences and PAG subregions that loaded similarly on a factor (Table S2). For factors 1 and 2, the pairwise correlations showed that activity in the left caudal ventrolateral region was negatively correlated with self-reported anger ($r = -0.62$, $P < 0.05$), and activity in the right caudal ventrolateral region was negatively correlated with arousal to the aversive images ($r = -0.53$, $P < 0.05$). These findings suggest that feelings of anger and arousal may emerge with diminishing activity in ventrolateral "passive-coping" columns. For factor 3, greater activity in the rostral lateral region was correlated with self-reported sadness in response to the aversive images ($r = 0.53$, $P < 0.05$). Although sadness is considered a prototypically low-arousal emotion (33), studies also have identified high-arousal and approach-oriented forms of sadness (34, 35), which may occur robustly with the aversive-image stimuli used here (36). As such, factor 3 suggests that feelings of sadness also may involve greater activity in a lateral active-coping column. We reiterate, however, that these specific interpretations are speculative.

More generally, and consistent with recent conceptual and theoretical developments in emotion research (30, 32, 37), these findings suggest that mappings between subjective emotional experiences, active-/passive-coping responses that and activity in PAG subregions may vary with the particular experimental contexts involved and are unlikely to involve simple one-to-one formulations of specific emotions with active and passive behavioral coping strategies in nonhuman animals. Precisely where and how emotional experiences in humans map onto activity in PAG would be an important question for future research using the techniques we developed here.

## Discussion

Using high-field strength, high-resolution fMRI, we made four observations related to the human PAG. First, we observed definitive activation in the human PAG while participants passively viewed aversive images. Prior studies have been unable to correct for the partial-volume issues that blend signal from PAG with the aqueduct and surrounding brainstem nuclei. Second, segmenting the PAG into both radial and longitudinal subregions illustrated that activity during negative affect was not diffuse but was concentrated along a spiral pattern from ventrolateral caudal PAG to lateral and dorsomedial rostral PAG. This pattern mirrors functional and structural observations in nonhuman animals (20–23). Indeed, it bears a striking resemblance to the distribution of c-Fos expression in rodents upon the administration of anxiogenic drugs (22). Third, analyses on a voxel-by-voxel basis showed peak activations in caudal ventrolateral PAG and in rostral lateral PAG. These findings indicate that high-field strength neuroimaging can be used to discover, on the voxel level, the functional architecture of human PAG. Finally, we found that activity in these subregions responded differentially; functional activity in these subregions loaded on separate factors with distinct emotional experiences. Thus, although they were located only a few millimeters apart, variability in these voxels was functionally distinct.

The results of this study highlight several points for understanding functional activity in human PAG using neuroimaging. First, submillimeter high-resolution imaging (such as the 0.75-mm resolution used here) is critical to separate activity in the PAG from the high variability observed in the aqueduct. Imaging studies that use lower resolutions, inexact normalization procedures, or smoothing without extracting high-variability signal from the aqueduct beforehand are prone to partial-volume effects that blend these signals.

Second, this study stresses the importance of imaging functional activity at the resolution of the underlying circuitry. We observed that portions of the lateral and ventrolateral PAG contributed distinct sources of information while processing aversive stimuli. Thus, although the PAG showed greater activity overall during the viewing of aversive images, the psychological interpretation of this activity rests on which portions of the PAG are being engaged. Notably, our approach may be extended to isolate BOLD activity in nearby midbrain regions, such as the substantia nigra, red nucleus, colliculi, potentially the dorsal raphe nucleus, and others that also are known be involved in emotional and cognitive functions (see Fig. S4 for an example). Separating these sources of signal will help resolve whether activity in the vicinity of the PAG reflects activity within the PAG or these other, nearby structures.

Third, this method may be used to explore homologies between human and animal PAG and to extend PAG studies to the more complex emotional reactions present in humans but difficult to elucidate in animals. Animal models have shown that escapable and inescapable stressors elicit active- and passive-coping responses, respectively, and these responses are related to distinct subregions of the PAG. However, whether this finding also holds for humans in similarly threatening contexts is unknown. Equally important, however, is to examine how the human PAG functions across a variety of aversive and appetitive situations. People vary widely in the complex array of cognitive, behavioral, and affective responses they may have in response to a given stimulus. We observed that variability in emotional experiences also relates to activity in discrete subregions of the PAG (e.g., sadness and anger). This finding indicates a role for PAG in emotional experience in addition to its known role in visceromotor responses to threat.

More broadly, activity in the vicinity of the PAG has also been observed across a tremendous variety of human functions. For example, responses in the vicinity of the PAG have also been observed during cognitive and social cognitive functions that are not traditionally associated with the PAG, including perception, attention, memory, and language (Fig. S5 and ref. 12). However, whether—and if so, how—the functionality of PAG in fact contributes to these abilities in humans remains unclear. The methodology developed in this study allows for pinpointing activity to subregions of the PAG. Future research may discover, with precision, what role the PAG plays in humans across these many domains.

## Methods

**Participants.** Thirteen healthy, right-handed participants provided informed consent in accordance with guidelines set forth by the Partner's Health Institutional Review Board. They received US$40/h in compensation. Two participants were excluded because functional data could not be collected as the result of a hard drive failure (one subject) or poor image quality caused by ghosting (one subject). For one participant, data from only two of three runs were included because of a programming failure in the third run. The analyzed sample included 11 participants (five male, age range, 20–35 y).

**Task and Stimuli.** To elicit affective responses, participants were shown 30 highly aversive images and 30 neutral images sampled from a database of normed photographs [the International Affective Picture System (29)]. Images were organized into 17.5-s blocks consisting of five images of each type, each randomly sampled once during the block and presented for 2 s followed by variable interstimulus intervals of 0.5, 1, 1.5, 2, or 2.5 s. After each block of images, participants reported their emotional response to the set of images using a five-button response box with the emotion labels "Activated" (for arousal), "Angry," "Disgusted," "Sad," and "Scared" in a random order and a numbered scale from 0–4 in which "0" indicated none and "4" indicated very much of the affect or emotion. After the 16-s reporting period, the next image block commenced. In other blocks, participants viewed images from another stimulus set (for details: K. Kveraga http://nmr.mgh.harvard.edu/~kestas/affcon) that were not the focus of this analysis. Confirming the aversive intensity of the images, self-report measures indicated that subjects experienced greater anger [$t_{robust}$ (9) = 8.86, $P < 0.00001$], disgust ($t_{robust}$ [10) = 5.74, $P < 0.001$], sadness [$t_{robust}$ (10) = 3.96, $P < 0.01$], and fear [scared; $t_{robust}$ (10) = 4.60, $P < 0.001$], but did not increase self-reported arousal [activated; $t_{robust}$ (10) = 0.22, $P < 0.84$]. Self-reports of emotional experiences were not significantly correlated with each other (all $P$s > 0.08), suggesting that the measures contributed different sources of variability and were unlikely to be reduced to valence and arousal dimensions (see Table S2).

**Neuroimaging Parameters.** Gradient-echo echo-planar imaging BOLD-fMRI was performed on a 7-T Siemens MRI scanner (Siemens Healthcare). A custom-built 32-channel RF loop coil head array was used for reception. Transmit was provided by a custom-built detunable band-pass birdcage coil. The functional imaging used single-shot gradient-echo Echo Planar Imaging: echo time = 26 ms, repetition time = 3s, flip angle = 90°, number of slices = 40, slice orientation = oblique axial/coronal (slices were oriented approximately perpendicular to the aqueduct), nominal voxel size = 0.75 mm isotropic, gap between slices = 0 mm, field of view = 192 × 192 $mm^2$, number of repetitions = 90, GRAPPA acceleration factor = 4; echo spacing = 1.04 ms, effective echo spacing = 1.04 ms/4 = 0.26 ms, bandwidth = 1,148 Hz per pixel, partial Fourier in the phase encode direction: 6/8.

**Neuroimaging Analysis.** For initial preprocessing, neuroimaging data were realigned using the linear registration tool in the FMRIB Software Library (FSL) (38–40) software package, and the data were filtered through a high-pass temporal filter (100 s); data were not smoothed or normalized at this stage (similar to procedures in ref. 41). We then manually segmented the PAG and the aqueduct for each functional run to normalize data across subjects without introducing partial volume between the PAG and the aqueduct. Taking advantage of the high variability in signal from the aqueduct, we computed a variance map to guide the generation of an aqueduct mask (Fig. S1), which then was inspected manually. A 2.25-mm (three-voxel) dilation around the aqueduct defined the PAG, which then was inspected manually. Resulting PAG masks ranged from 8.25–12 mm longitudinally across participants. PAG masks were applied to the functional data to include signal from the PAG and to exclude signal from the aqueduct and surrounding tissue.

General linear models consisting of regressors of the onsets for each image category convolved with the double gamma hemodynamic response function along with their first-order temporal derivatives were applied to the averaged PAG signal (for examining the undivided PAG) or to each voxel (for examining subregions) using robust regressions (42) to minimize the influence of outliers. Across scans, the maximal relative displacement in motion had a median of 0.39 mm, an interquartile range of 0.29–0.61 mm, and minimum/maximum range of 0.15–1.45 mm. To account for fluctuations in response caused by motion, motion parameters were included in the model, and robust regressions were used in calculations of paired $t$ tests and correlations to limit the influence of outliers upon the statistical analyses.

To examine PAG subregions, a custom PAG template was generated to align data across participants (Fig. S1). First, each slice within each individual PAG mask was centered to reshape it into a cylinder. Second, a template mask was generated by summing across individual maps and including voxels that showed overlaps by at least two participants' masks. Registration of individual masks to the template mask was performed using FSL's FLIRT with trilinear interpolation. The parameters from these transformations then were applied to the functional data (for which aqueduct and surrounding tissue signal already had been masked out). The resulting maps were smoothed minimally by applying a 1 × 1 × 1 mm Gaussian kernel [Statistical Parametric Mapping 8 software (43)].

For the mask-based analyses, the PAG template was divided radially (six segments) and rostrocaudally (six segments), and parameter estimates for aversive and neutral image viewing conditions were averaged across voxels within these segments for each participant. A repeated-measures ANOVA was performed to test whether functional activity was segregated to specific subregions of the PAG. Follow-up robust paired $t$ tests were performed to test whether activations were concentrated in rostrocaudal and radial organizations of PAG. For voxelwise analyses, robust $t$ tests were calculated for

each voxel within the PAG template, and familywise error correction was determined by using FSL's tfce. Resulting $P_{tfce}$ values and uncorrected $t$ and $P$ values for comparison are reported only for voxels that met significance. There was no uncorrected threshold for voxelwise analyses.

**Factor Analysis.** The central purpose of the exploratory factor analysis was to examine whether PAG subregions identified in the voxelwise analyses shared variability and loaded similarly across factors or whether they contained meaningfully different variability and loaded on separate factors. Our central purpose was not to identify precise relationships between emotional experiences and activity in PAG subregions, although these relationships are of interest for future work using the technique we developed here. Our goals are generally consistent with suggested guidelines for exploratory factor analyses with small samples ($n < 20$) as described recently (44).

Spherical masks (0.7-mm radius) were created centered on peak voxels for the three activations that reached significance in the voxelwise analyses. The difference in parameter estimates for the comparison of aversive and neutral stimulus conditions was extracted for each participant. Self-reported measures of emotional responses to the aversive vs. neutral blocks of images were averaged for each participant. These measures were submitted together to a principle components analysis with direct oblimin rotation, which does not force orthogonal factor solutions. Using an orthogonal rotation did not alter the pattern of results. Communalities were in the moderate to high range (minimum = 0.62, maximum = 0.88) and indicated no Heywood cases. The analysis revealed three factors with eigenvalues above 1.

**ACKNOWLEDGMENTS.** We thank Jochen Weber for assistance with figures. This research was carried out in part at the Athinoula A. Martinos Center for Biomedical Imaging at the Massachusetts General Hospital using resources provided by the Center for Functional Neuroimaging Technologies, P41EB015896, a P41 Regional Resource supported by the National Institute of Biomedical Imaging and Bioengineering, National Institutes of Health (NIH). This work involved the use of instrumentation supported by the NIH Shared Instrumentation Grant Program Grants S10RR023043, S10RR019307, and S10RR023401. This work also was funded by NIH Director's Pioneer Award DP1OD003312 (to L.F.B.), Army Research Institute Contract W5J9CQ-11-C-0046 (to L.F.B.), and by National Institute of Mental Health Grants 2R01MH076136 and R21MH082308 (both to T.D.W.). The views, opinion, and/or findings contained in this article are solely those of the authors and should not be construed as an official Department of the Army or Department of Defense position, policy, or decision.

1. Bandler R, Keay KA, Floyd N, Price J (2000) Central circuits mediating patterned autonomic activity during active vs. passive emotional coping. *Brain Res Bull* 53(1): 95–104.
2. Behbehani MM (1995) Functional characteristics of the midbrain periaqueductal gray. *Prog Neurobiol* 46(6):575–605.
3. Fanselow MS (1991) The midbrain periaqueductal gray as a coordinator of action in response to fear and anxiety. *The Midbrain Periaqueductal Gray Matter*, eds Depaulis A, Bandler R (Plenum, New York), Vol 105, pp 151–173.
4. Bandler R, Shipley MT (1994) Columnar organization in the midbrain periaqueductal gray: Modules for emotional expression? *Trends Neurosci* 17(9):379–389.
5. Panksepp J (2011) The basic emotional circuits of mammalian brains: Do animals have affective lives? *Neurosci Biobehav Rev* 35(9):1791–1804.
6. Drevets WC (2001) Neuroimaging and neuropathological studies of depression: Implications for the cognitive-emotional features of mood disorders. *Curr Opin Neurobiol* 11(2):240–249.
7. Cechetto DF, Shoemaker JK (2009) Functional neuroanatomy of autonomic regulation. *Neuroimage* 47(3):795–803.
8. Tracey I (2005) Nociceptive processing in the human brain. *Curr Opin Neurobiol* 15(4): 478–487.
9. Fields H (2004) State-dependent opioid control of pain. *Nat Rev Neurosci* 5(7): 565–575.
10. Bittar RG, et al. (2005) Deep brain stimulation for pain relief: A meta-analysis. *J Clin Neurosci* 12(5):515–519.
11. Borsook D (2012) Neurological diseases and pain. *Brain* 135(Pt 2):320–344.
12. Linnman C, Moulton EA, Barmettler G, Becerra L, Borsook D (2012) Neuroimaging of the periaqueductal gray: State of the field. *Neuroimage* 60(1):505–522.
13. Mobbs D, et al. (2007) When fear is near: Threat imminence elicits prefrontal-periaqueductal gray shifts in humans. *Science* 317(5841):1079–1083.
14. Tracey I, et al. (2002) Imaging attentional modulation of pain in the periaqueductal gray in humans. *J Neurosci* 22(7):2748–2752.
15. Buhle JT, et al. (2013) Common representation of pain and negative emotion in the midbrain periaqueductal gray. *Soc Cogn Affect Neurosci* 8(6):609–616.
16. Kober H, et al. (2008) Functional grouping and cortical-subcortical interactions in emotion: A meta-analysis of neuroimaging studies. *Neuroimage* 42(2):998–1031.
17. Lindquist KA, Wager TD, Kober H, Bliss-Moreau E, Barrett LF (2012) The brain basis of emotion: A meta-analytic review. *Behav Brain Sci* 35(3):121–143.
18. Lund TE, Madsen KH, Sidaros K, Luo WL, Nichols TE (2006) Non-white noise in fMRI: Does modelling have an impact? *Neuroimage* 29(1):54–66.
19. Dagli MS, Ingeholm JE, Haxby JV (1999) Localization of cardiac-induced signal change in fMRI. *Neuroimage* 9(4):407–415.
20. Moss MS, Basbaum AI (1983) The peptidergic organization of the cat periaqueductal gray. II. The distribution of immunoreactive substance P and vasoactive intestinal polypeptide. *J Neurosci* 3(7):1437–1449.
21. Moss MS, Glazer EJ, Basbaum AI (1983) The peptidergic organization of the cat periaqueductal gray. I. The distribution of immunoreactive enkephalin-containing neurons and terminals. *J Neurosci* 3(3):603–616.
22. Singewald N, Sharp T (2000) Neuroanatomical targets of anxiogenic drugs in the hindbrain as revealed by Fos immunocytochemistry. *Neuroscience* 98(4):759–770.
23. Rizvi TA, Ennis M, Behbehani MM, Shipley MT (1991) Connections between the central nucleus of the amygdala and the midbrain periaqueductal gray: Topography and reciprocity. *J Comp Neurol* 303(1):121–131.
24. Keil B, Triantafyllou C, Hamm M, Wald L (2010) Design optimization of a 32-channel head coil at 7 T. *Proceedings of the International Society of Magnetic Resonance in Medicine* (Stockholm), p 1493.
25. Wiggins GC, et al. (2006) 32-channel 3 Tesla receive-only phased-array head coil with soccer-ball element geometry. *Magn Reson Med* 56(1):216–223.
26. Duyn JH (2012) The future of ultra-high field MRI and fMRI for study of the human brain. *Neuroimage* 62(2):1241–1248.
27. Uğurbil K, et al. (1999) Functional mapping in the human brain using high magnetic fields. *Philos Trans R Soc Lond B Biol Sci* 354(1387):1195–1213.
28. Yacoub E, et al. (2001) Imaging brain function in humans at 7 Tesla. *Magn Reson Med* 45(4):588–594.
29. Lang PJ, Bradley MM, Cuthbert BN (2008) International affective picture system (IAPS): Affective ratings of pictures and instruction manual. Technical Report A-8. (University of Florida, Gainesville, FL).
30. Barrett LF (2006) Solving the emotion paradox: Categorization and the experience of emotion. *Pers Soc Psychol Rev* 10(1):20–46.
31. Barrett LF, et al. (2007) Of mice and men: Natural kinds of emotions in the mammalian brain? A response to Panksepp and Izard. *Perspect Psychol Sci* 2(3):297–311.
32. Barrett LF (2012) Emotions are real. *Emotion* 12(3):413–429.
33. Russell JA, Barrett LF (1999) Core affect, prototypical emotional episodes, and other things called emotion: Dissecting the elephant. *J Pers Soc Psychol* 76(5):805–819.
34. Witvliet CV, Vrana SR (1995) Psychophysiological responses as indices of affective dimensions. *Psychophysiology* 32(5):436–443.
35. Wilson-Mendenhall CD, Barrett LF, Barsalou LW (2013) Neural evidence that human emotions share core affective properties. *Psychol Sci* 24(6):947–956.
36. Mikels JA, et al. (2005) Emotional category data on images from the International Affective Picture System. *Behav Res Methods* 37(4):626–630.
37. Wilson-Mendenhall CD, Barrett LF, Simmons WK, Barsalou LW (2011) Grounding emotion in situated conceptualization. *Neuropsychologia* 49(5):1105–1127.
38. Jenkinson M, Beckmann CF, Behrens TE, Woolrich MW, Smith SM (2012) Fsl. *Neuroimage* 62(2):782–790.
39. Smith SM, et al. (2004) Advances in functional and structural MR image analysis and implementation as FSL. *Neuroimage* 23(Suppl 1):S208–S219.
40. Woolrich MW, et al. (2009) Bayesian analysis of neuroimaging data in FSL. *Neuroimage* 45(1, Suppl):S173–S186.
41. Satpute AB, Mumford JA, Naliboff BD, Poldrack RA (2012) Human anterior and posterior hippocampus respond distinctly to state and trait anxiety. *Emotion* 12(1): 58–68.
42. Wager TD, Keller MC, Lacey SC, Jonides J (2005) Increased sensitivity in neuroimaging analyses using robust regression. *Neuroimage* 26(1):99–113.
43. Friston KJ, Ashburner JT, Kiebel SJ, Nichols TE, Penny WD (2011) *Statistical Parametric Mapping: The Analysis of Functional Brain Images* (Academic, London).
44. de Winter J, Dodou D, Wieringa P (2009) Exploratory factor analysis with small sample sizes. *Multivariate Behav Res* 44(2):147–181.

# Supporting Information

Satpute et al. 10.1073/pnas.1306095110

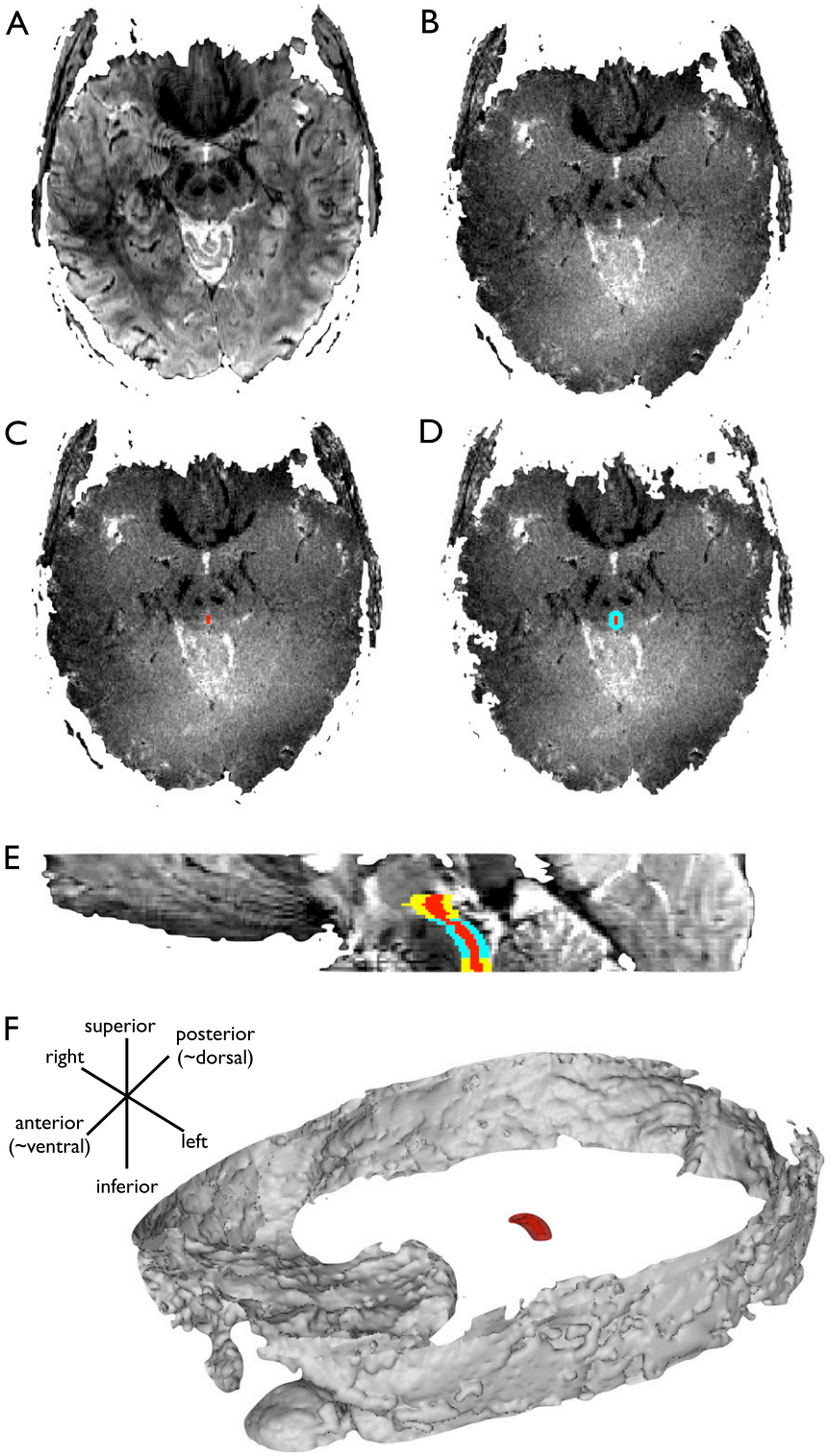


**Fig. S1.** Isolating the periaqueductal gray (PAG). PAG masks were generated directly from the functional data. Standard imaging procedures introduce partial-volume effects that merge signal from the aqueduct with signal from the PAG because of large voxel sizes, imprecise normalization, and smoothing

Legend continued on following page

procedures. The figure illustrates how ultra-high resolution 7-T neuroimaging and a procedure for generating targeted masks can be used to isolate signal from the PAG. (*A*) The mean image of a single functional run illustrates the advantage of high-resolution scanning at 7 T by clearly showing the PAG and other subcortical structures including the red nucleus and substantia nigra. (*B*) The variability image of the functional scan clearly distinguishes the aqueduct (in white) from the surrounding PAG (in gray). (*C*) A mask is generated for aqueduct as shown in red using the variability image for each functional run. (*D*) The PAG is identified as surrounding the aqueduct, shown in blue, using a dilation of three voxels (2.25 mm) for each functional run. Masks were inspected visually and edited manually as needed. (*E*) A sagittal slice showing the aqueduct in red and PAG in blue (yellow regions extended beyond the PAG and were removed manually). (*F*) An example of a PAG mask for one run depicted in 3D.

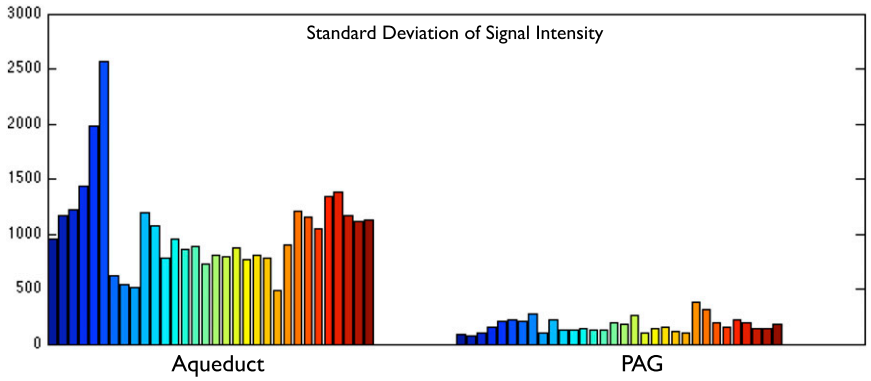


**Fig. S2.** Comparison of signal variability in the PAG and the aqueduct. The SD of signal is plotted for 32 functional runs for signal averaged within masks for the aqueduct and the PAG. On average and across runs, the SD of signal in the aqueduct is 6.11 times greater than in the PAG (or 36 times greater in variance). Signal in the aqueduct can mask findings because of added noise and also can create artifactual observations attributed to the PAG because of the influence of heart rate on cerebrospinal fluid flow (1).

1. Dagli MS, Ingeholm JE, Haxby JV (1999) Localization of cardiac-induced signal change in fMRI. *Neuroimage* 9(4):407–415.

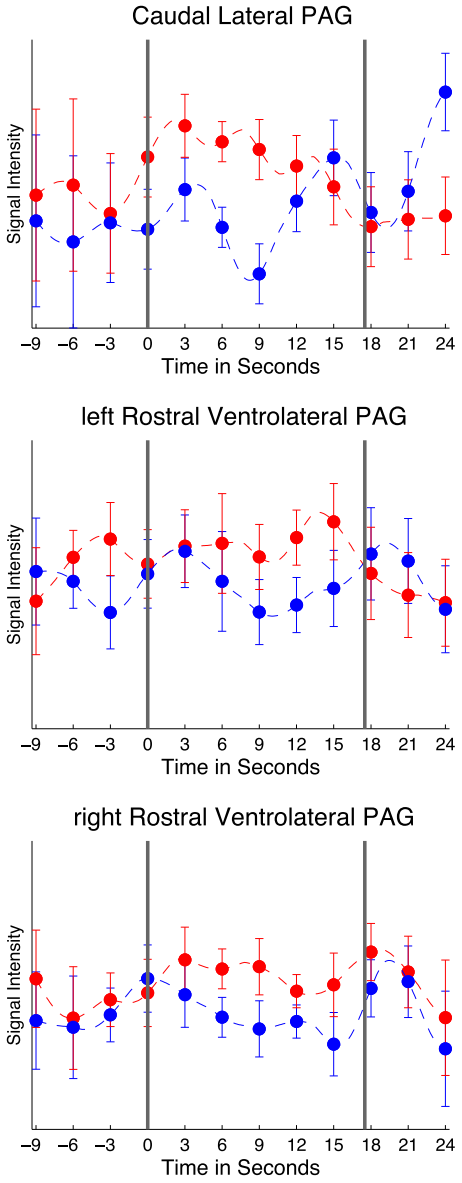


**Fig. S3.** Sample mean time-course plots from single voxels in the PAG. Raw signal intensity was extracted from each functional scan for each subject for the three peak voxels: the caudal lateral PAG (*Top*), the left rostral ventrolateral PAG (*Middle*), and the right rostral ventrolateral PAG (*Bottom*). The first gray bar at time point 0 marks the onset of the block of images (either aversive or neutral), which lasted for 17.5 s; the second bar marks the offset of the block. SE bars for within subject effects show the variability of the differences between conditions over time points. The plots demonstrate that, on average, the increase in signal intensity is greater during aversive-image viewing (red lines) than during neutral-image viewing (blue lines). Images were presented in separate blocks, but activity is overlaid here for ease of comparison. Intriguingly, the averaged hemodynamic responses appear slightly different among the regions, a finding that may be of interest for future investigations that optimize detecting the properties of the hemodynamic response to various kinds of affective stimuli.

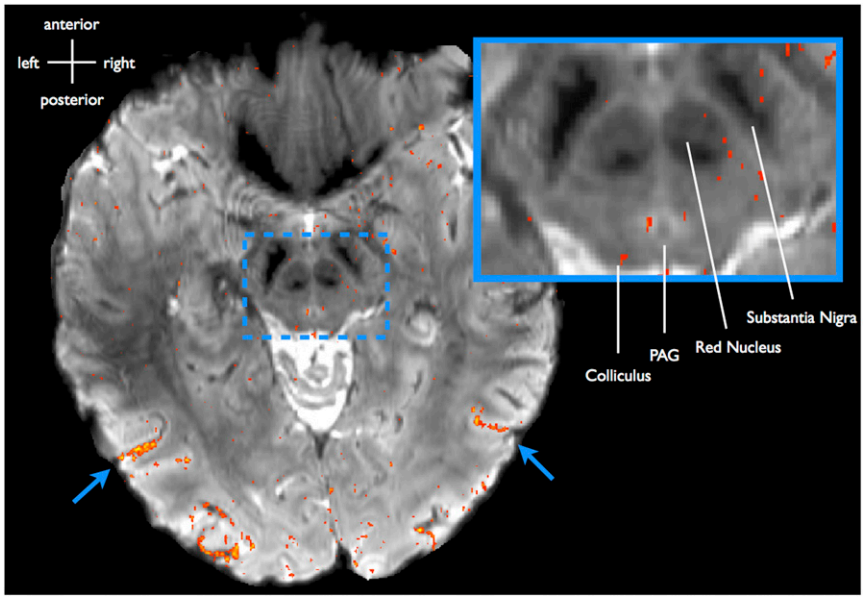


**Fig. S4.** Functional activity in brainstem nuclei as revealed by neuroimaging at 7 T. The figure illustrates the greater precision obtained when using high-field strength and high-resolution imaging. The figure is provided for illustrative purposes only and does not reflect the precise methods used to acquire signal from the PAG specifically (which are illustrated in Fig. S1). The underlay is the mean functional image for a single participant. The overlay is functional activity during the viewing of aversive relative to neutral images for that participant (uncorrected, $P < 0.05$). Blue arrows point to functional activations that track closely with the particular morphology of sulci and gyri of the participant's lateral occipital and occipitotemporal cortex. The enlarged view in the blue box shows separation among brainstem nuclei directly in the functional scans. The colliculi, the PAG, the red nucleus, and substantia nigra are visible landmarks that also may be used to triangulate activation in adjacent nuclei. The functional parameters were tuned to maximize signal in the PAG. Adjustments would be required to maximize signal in the red nucleus and substantia nigra (which are higher in iron content and may improve with a reduced echo time) and possibly in other brainstem nuclei.

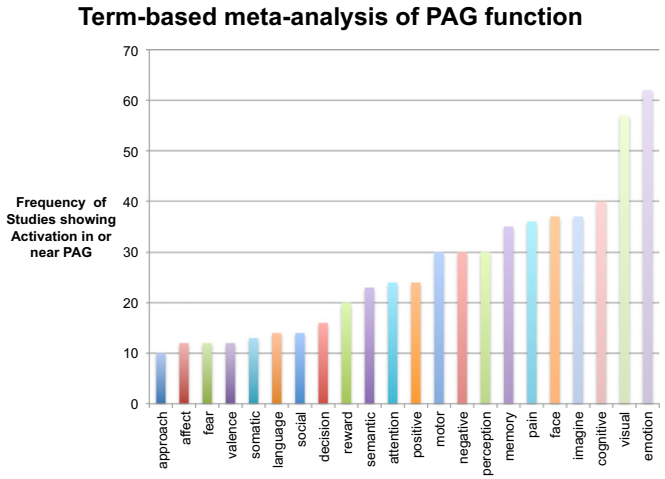


**Fig. S5.** Term-based meta-analysis of PAG function from functional MRI and PET studies. Neuroimaging studies routinely show activity in the vicinity of the PAG across a broad array of domains, suggesting that regulation of homeostasis may be important to a broad range of psychological events. We used a term-based summary map from a database of more than 6,000 neuroimaging studies (NeuroSynth) (1) and identified 145 studies that showed activation in or near the PAG. NeuroSynth indexes the psychological content domains on which these studies focused based on the frequency counts of words. The bar plot shows the number of articles that focused on various kinds of psychological content and also show activity in or near PAG. Of the 145 total studies, studies examining "emotion" were most frequent; however, studies investigating a variety of other psychological contents also frequently engage voxels in the vicinity of the PAG. The standard neuroimaging methods used in these studies cannot pinpoint whether the PAG is in fact frequently engaged in these domains.

1. Yarkoni T, Poldrack RA, Nichols TE, Van Essen DC, Wager TD (2011) Large-scale automated synthesis of human functional neuroimaging data. *Nat Methods* 8(8):665–670.

**Table S1. Pattern matrix from factor analysis**

| Measure | Factor 1 | Factor 2 | Factor 3 |
|---|---|---|---|
| Angry | −0.19 | **0.89** | −0.21 |
| Aroused | **0.73** | −0.25 | 0.28 |
| Disgusted | **0.82** | 0.18 | 0.12 |
| Sad | 0.18 | 0.03 | **0.89** |
| Scared | **0.72** | 0.32 | 0.01 |
| PAG, left rostrallateral | −0.09 | −0.11 | **0.83** |
| PAG, left caudal ventrolateral | −0.33 | **-0.85** | −0.07 |
| PAG, right caudal ventrolateral | **-0.73** | 0.44 | 0.34 |

The table presents the pattern matrix from a factor analysis involving participants' self-reported emotional experiences and neural activity in PAG clusters for aversive vs. neutral images. A principle components extraction with direct oblimin rotation was performed on these measures. Three factors were extracted with eigenvalues above 1, accounting for 35, 24, and 18% of the variability, respectively, indicating that variability was spread fairly evenly, given the principle components extraction method. Communalities were in the moderate to high range (0.62–0.88), indicating no Heywood cases. Factor loadings at 0.72 and above are in bold. Instead of loading similarly across factors or uncovering a single-factor solution, the analysis suggests that the PAG clusters loaded on separate factors. Moreover, each factor comprised activity in a PAG cluster and a self-report measure of emotion. Factor 1 involved the left caudal ventrolateral PAG and the emotions disgust, arousal, and fear. Factor 2 involved the right caudal ventrolateral PAG and the emotion anger. Factors 1 and 2 suggest that feelings of disgust, arousal, fear, and anger emerge as activity in ventrolateral passive coping columns diminishes. Factor 3 involved the rostral lateral PAG and sadness. Although sadness is considered a prototypically low-arousal emotion, studies also have identified high-arousal and approach-oriented forms of sadness, which may be more likely to occur with the aversive images used here (see main text). As such, Factor 3 suggests that more feelings of sadness may relate with greater activity in the ventrolateral active coping column. In general, these findings suggest that mappings between subjective emotional experiences, active-/passive-coping responses, and activity in PAG subregions may vary with the particular experimental contexts involved and are unlikely to involve simple one-to-one formulations of specific emotions with active and passive behavioral coping strategies in nonhuman animals.

**Table S2. Correlation between emotional experience and PAG subregions**

| | Angry | Activated | Disgusted | Sad | Scared |
|---|---|---|---|---|---|
| Angry | | | | | |
| Activated | −0.38 | | | | |
| Disgusted | −0.04 | 0.45 | | | |
| Sad | −0.17 | 0.51 | 0.36 | | |
| Scared | −0.03 | 0.29 | 0.37 | 0.02 | |
| PAG, left rostral lateral | −0.28 | −0.10 | 0.08 | **0.53** | 0.00 |
| PAG, left caudal ventrolateral | **−0.62** | 0.06 | −0.38 | −0.22 | −0.25 |
| PAG, right caudal ventrolateral | 0.48 | **−0.53** | −0.14 | 0.10 | −0.39 |

The table presents the correlation matrix (obtained using robust correlations for outlier correction) between emotional experience reports and between emotional experience with PAG subregions identified from the voxelwise analyses. Correlations in bold were significant at $P < 0.05$ (uncorrected). The factor analysis indicates that variability in activity in PAG subregions loaded on three separate factors. Each factor also was associated with different emotional experience reports. The results suggest that although subregions of PAG were only millimeters apart, they appear to operate in different functional circuits based on showing low intercorrelations among each other (as described in the main text) and differential patterns of factor loadings and correlations with the emotional experience reports. Greater activity in the rostral lateral region was correlated with self-reported sadness in response to the aversive images ($r = 0.53$, $P < 0.05$), whereas activity in the caudal ventrolateral regions were not (left caudal ventrolateral: $r = 0.10$, $P < 0.4$; right caudal ventrolateral: $r = -0.22$, $P < 0.3$). Alternatively, greater activity in the left caudal ventrolateral region was negatively correlated with self-reported anger ($r = -0.62$, $P < 0.05$), and activity in the right caudal ventrolateral region was negatively correlated with arousal to the aversive images ($r = -0.53$, $P < 0.05$). Activity in the right rostral lateral region was not associated with self-reported anger ($r = -0.28$, $P < 0.3$) or with arousal ($r = -0.10$, $P < 0.4$; Table S1). Robust regressions were used for outlier correction.